

# Conceptual Design of the FCC-hh Dipole Circuits With Integrated CLIQ Protection System

Marco Prioli , Bernhard Auchmann , Lorenzo Bortot , Michał Maciejewski , Tiina Salmi ,  
and Arjan Verweij 

**Abstract**—The Future Circular Collider (FCC-hh) project is a conceptual study whose goal is to design the successor of the Large Hadron Collider, increasing the collision energy from 14 to 100 TeV. The energy stored in the 16-T superconducting dipole magnets and the length of the sectors composing the 100-km FCC tunnel are considerably larger than those in present accelerators. This means that the energy stored in the FCC-hh dipole circuit is likely to be much higher than that in existing superconducting circuits. In the case of magnet quenches or faults, the circuit needs to be protected, i.e., its energy needs to be rapidly dissipated without inducing excessive voltages in the magnet chain. This article proposes a conceptual design for the FCC-hh dipole circuit, which satisfies the constraint of the maximum allowable voltage-to-ground and fulfills additional requirements related to the FCC-hh operation and tunnel layout. A compromise among the considered requirements leads to a relatively simple circuit layout and a large number of circuits for the entire machine. The behavior of the proposed circuit during the critical fast power abort phase is simulated through a numerical model, which covers the electrical circuit domain and the electrothermal magnet domain. Each FCC-hh dipole magnet is protected by means of the coupling-loss-induced quench (CLIQ) protection system, which also acts at the circuit level. The simulations predict severe voltage oscillations in the FCC-hh dipole circuits that may pose a problem for the quench detection system. The simulations also show that the severity of the oscillations is not due to the presence of CLIQ. This protection system can be integrated into the proposed circuit layout and represents an effective protection system for the entire string of FCC-hh dipole magnets.

**Index Terms**—Coupling-loss induced quench (CLIQ), Future Circular Collider (FCC), quench protection, superconducting circuits.

Manuscript received March 20, 2019; revised June 6, 2019; accepted June 10, 2019. Date of publication September 27, 2019; date of current version November 4, 2019. This work was performed at CERN. This article was recommended by Associate Editor C. Luongo. (Corresponding author: Marco Prioli.)

M. Prioli was with Machine Protection and Electrical Integrity Group, Technology Department CERN, 1211 Geneva, Switzerland. He is now with Accelerators and Applied Superconductivity Laboratory, National Institute for Nuclear Physics, 20133 Milano, Italy (e-mail: marco.prioli@mi.infn.it).

B. Auchmann is with Machine Protection and Electrical Integrity Group, Technology Department, CERN, 1211 Geneva, Switzerland, and also with Paul Scherrer Institute, 5232 Villigen, Switzerland.

L. Bortot and A. Verweij are with Machine Protection and Electrical Integrity Group, Technology Department, CERN, 1211 Geneva, Switzerland.

M. Maciejewski is with Machine Protection and Electrical Integrity Group, Technology Department, CERN, 1211 Geneva, Switzerland, and also with the Łódź University of Technology, 90-924 Łódź, Poland.

T. Salmi is with the Tampere University of Technology, 33101 Tampere, Finland.

Color versions of one or more of the figures in this article are available online at <http://ieeexplore.ieee.org>.

Digital Object Identifier 10.1109/TASC.2019.2931172

## I. INTRODUCTION

THE quench protection of superconducting dipole magnets of the Future Circular Collider (FCC-hh) was integrated into the 16-T development program [1]. The adopted protection criterion is that the maximum voltage-to-ground and hot-spot temperature developed in the magnet coils in the case of a quench must be below safe limits [1]. The voltage-to-ground depends on the layout of the circuit employed to feed the magnets. Fig. 1 shows a simplified schematic of the Large Hadron Collider (LHC) dipole circuit featuring 154 dipole magnets in series ( $M_k$ , with  $k = 1, \dots, 154$ ). When a magnet quenches, a fast power abort (FPA) is triggered to dissipate the circuit energy rapidly and safely. Both passive and active protection systems are activated at the circuit level. Among the passive systems, a protection diode is connected in parallel to each magnet to bypass the circuit current after the quench. Concerning the active systems, the power converter (PC) is turned OFF, and its crowbar is fired to create a continuity path for the circuit current. The switches  $SW_{EE1}$  and  $SW_{EE2}$  of the energy extraction (EE) systems are opened to create a resistive voltage and discharge the current.

During the FPA phase, the circuit shows the highest voltages-to-ground. In particular, the maximum voltage drop from the magnet coils to ground is composed of two contributions

$$V_{\text{magnet,gnd}} = V_{\text{magnet,circuit}} + V_{\text{circuit,gnd}} \quad (1)$$

where  $V_{\text{magnet,circuit}}$  is the voltage drop from the magnet coils to the input current lead connecting the magnet to the rest of the circuit (nodes  $k_{in}$ , with  $k = 1, \dots, 154$  in Fig. 1) and  $V_{\text{circuit,gnd}}$  is the voltage drop from the input lead to the grounding point (node 0 in Fig. 1). The first contribution is the internal voltage distribution of the magnet, and it depends on the unbalance of the inductive and resistive voltage developed during a quench. This is also true for the second contribution, for which the inductive voltage is due to other magnets connected to the circuit, and the resistive voltage is due to EE systems.

In the 16-T magnet development program, a maximum budget of 1.2 kV was assigned to  $V_{\text{magnet,circuit}}$  and 1.3 kV to  $V_{\text{circuit,gnd}}$  for the healthy circuit. For accelerator circuits with multiple magnets connected in series, these two contributions develop on different time scales. As an example, for the circuit of Fig. 1, the time constant of all electrical variables at the magnet level is in the order of 100 ms, while the one at the circuit level is in the order of 100 s. Unfortunately, during the development of the internal magnet voltage, the circuit voltage is at its peak, and

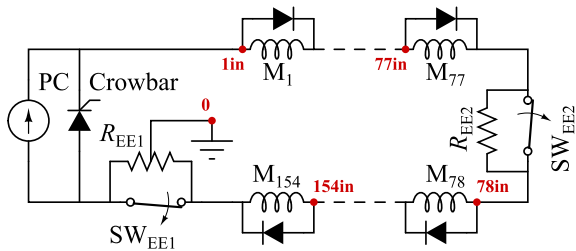


Fig. 1. Schematic of the LHC dipole circuit.

therefore, the maximum total voltage-to-ground is the sum of the two contributions. Following these considerations, the budget for the total voltage-to-ground ( $V_{\text{magnet,gnd}}$ ) equals 2.5 kV.

The quench protection at the magnet level is already addressed in [2]–[4]. The main outcome of this study is that two different active protection systems can be effectively employed to limit the internal voltage-to-ground and hot-spot temperature below safe limits, namely the quench heaters [5] and the coupling-loss-induced quench (CLIQ) protection system [6]. As CLIQ guarantees higher margins and offers a simpler design of the protection system, it was indicated as the baseline option. A CLIQ unit consists of a charged capacitor bank that generates oscillations in the magnet transport current that deposit ac losses in the conductor. It acts both at the magnet level (spreading the normal zone after a quench and developing resistance and voltage in the magnet coils) and the circuit level (being electrically connected to the circuit). The companion paper [2] discusses extensively the effect of CLIQ at the magnet level, along with the identification of the CLIQ configurations ensuring that the internal voltage and hot-spot temperature developed in the case of a quench are below safe limits.

This article addresses the protection of FCC-hh dipole magnets at the circuit level. The first topic that is discussed is the design of a circuit featuring a maximum voltage-to-ground during the FPA of 1.3 kV and fulfilling additional constraints related to the FCC-hh operation and tunnel layout. Then, the effect of CLIQ on the circuit protection is discussed by means of numerical simulations of the quench and the subsequent FPA phase. To this end, a numerical circuit model based on netlists is developed in Cadence PSpice, and a finite-element electrothermal model of an FCC-hh dipole magnet protected by CLIQ is developed in COMSOL [7]. These models are then coupled by means of the STEAM cosimulation framework recently developed at CERN [8] that allows performing a consistent simulation through the cooperation of different models. More details on STEAM can be found in [8]–[10]. The cosimulation of the magnet and circuit domains is needed due to the coupling introduced by CLIQ.

## II. CIRCUIT DESIGN

### A. Critical Protection Aspects

The design and protection of the FCC-hh dipole circuits is an important part of the 16-T development program [1] because the energy stored in the magnets and the length of the sectors composing the 100 km tunnel are much higher than

TABLE I  
PARAMETERS OF THE FOUR FCC-HH DIPOLE MAGNET DESIGNS COMPARED WITH THE ONES OF LHC MB MAGNETS

	Nominal current $I_{\text{nom}}$ [kA]	Stored energy @ $I_{\text{nom}}$ (Two apertures) [MJ]	Inductance $L_{\text{mag}}$ [mH]
FCC $\cos\theta$ (baseline)	11.4	37	570
FCC block-coil	10.1	38	730
FCC common-coil	16.1	44	340
FCC canted $\cos\theta$	18.0	46	280
LHC MB	11.9	7	98

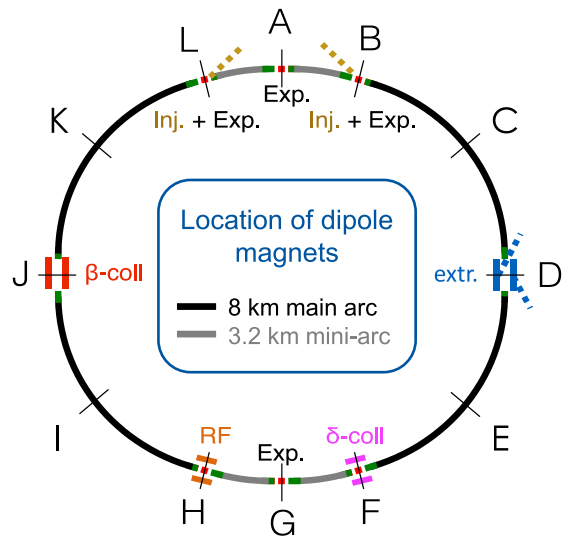


Fig. 2. Location of the dipole magnets in the FCC-hh layout.

those in present accelerators. Table I shows the nominal current and stored energy for the four options presently considered for the dipole magnets [1] and for the LHC main bending (MB) magnets. The  $\cos\theta$  magnet, selected as the baseline FCC-hh dipole design, has a nominal current similar to the LHC MB magnet but approximately five times higher stored energy.

In this article, the design and protection of FCC-hh circuits will be discussed considering the parameters of the baseline option. When the alternative magnet designs are also considered, two groups can be identified:  $\cos\theta$  and block-coil designs have similar nominal currents and stored energies and, therefore, result in the same circuit layout. Common-coil and canted  $\cos\theta$  options have higher stored energy, which is a clear disadvantage for the circuit protection, and lower inductance, which is instead an advantage for the fast discharge. It will be shown that the proposed circuit layout is modular, i.e., it can be easily adapted to these different features.

As shown in Fig. 2, FCC-hh dipole magnets are located in arcs of different lengths: the 8-km-long main arc that interconnects two access points and the 3.2-km-long mini-arcs close to the experiments. As shown in Table II, the number of dipole magnets located in the FCC-hh main arc is, due to the arc length, almost three times higher than the number of magnets in the LHC arc. This is the second critical aspect in the design of the FCC-hh circuits, as the LHC layout shown in Fig. 1 would lead

TABLE II  
PARAMETERS OF THE TWO FCC-hh ARC TYPES COMPARED WITH THE ONES  
OF THE LHC ARC

	Length [km]	Number	Number of magnets
FCC main arc	8	8	438
FCC mini-arc	3.2	4	180
LHC arc	3	8	154

to unacceptable voltages-to-ground when applied to the long FCC-hh arcs. The circuit design is here developed for the most critical main arcs. It will be shown that the proposed circuit architecture can be directly applied also to the mini-arcs.

### B. Design Strategy

Let us first consider the possibility of extrapolating the layout of the LHC dipole circuit shown in Fig. 1 to the FCC-hh main arcs. Following this strategy, all the magnets in one arc are connected in series, and two EE systems are located at the circuit ends. The grounding point is located in the middle of the first EE system (EE1) to reduce the maximum voltage-to-ground. The value of the resistance is selected such that the time constant for the fast circuit discharge is in the order of 100 s. The maximum voltage-to-ground during the FPA can be easily calculated as

$$\hat{V}_{\text{circuit, gnd}} = I_{\text{nom}} \frac{R_{\text{EE}}}{2} = \frac{I_{\text{nom}} N_{\text{mag}} L_{\text{mag}}}{2 N_{\text{EE}} \tau} \cong 7 \text{ kV} \quad (2)$$

where  $I_{\text{nom}}$  and  $L_{\text{mag}}$  are the magnet nominal current and inductance, respectively,  $R_{\text{EE}}$  and  $N_{\text{EE}}$  are the resistance and the number of EE systems, respectively,  $N_{\text{mag}}$  is the number of magnets in series in the circuit, and  $\tau$  is the discharge time constant. The factor 2 in the formula is due to the aforementioned selection of the grounding point. Equation (2) gives a maximum voltage-to-ground for the considered circuit of 7 kV that is much higher than the 1.3-kV budget.

Two different strategies can be applied to reduce the voltage-to-ground, namely to decrease the unbalance of inductive and resistive voltage. The first one is to keep the length of the circuit constant and increase the number of EE systems distributing them along the circuit, i.e., along the accelerator tunnel. The second one is to reduce the circuit length by splitting the long circuit into a number of independent circuits and equip each circuit with a single EE system. The second strategy is applied in this article, as it leads to a number of advantages. First of all, it reduces the energy stored in each circuit, limiting the possible consequences of fault scenarios. Second, it allows us to position all EE systems on one side of the arc, i.e., close to the access point. EE systems are bulky devices often subject to maintenance operations. The possibility of placing them close to the access points optimizes the use of space in the tunnel and simplifies their maintenance. The main disadvantages of the sectorization strategy are the multiplication of the electrical feedthroughs and busbars (two per circuit) and of the PCs (one per circuit). These drawbacks can be mitigated by the possibility of installing a

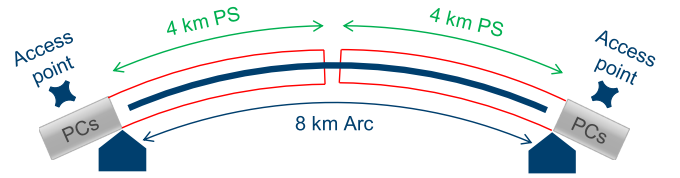


Fig. 3. Definition of the FCC-hh PS. Location of PCs and energy extractors (EEs) is also shown.

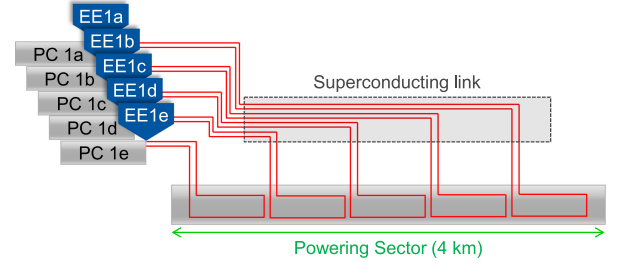


Fig. 4. Schematic of the dipole circuit architecture. Five circuits per PS are shown.

superconducting link in the tunnel and considering that high-power PCs have usually a modular structure. From this point of view, a single high-power PC is similar to several PCs with lower power. Moreover, the LHC experience proved that the possible synchronization issues among multiple converters can be effectively solved.

The FCC-hh powering sector (PS) is here defined as half of the 8-km arc, as shown in Fig. 3. Following the above considerations, each PS is further subdivided into multiple circuits, each equipped with a PC and a single EE system located close to the access points, as shown in Fig. 4. Since the length of the mini-arcs (3.2 km) is similar to that of the PS (4 km), a comparable number of circuits will be obtained for these two arcs. Considering the number of PS  $N_{\text{PS}} = 16$  and mini-arcs  $N_{\text{MA}} = 4$  in the machine and their length ratio  $l_{\text{MA}}/l_{\text{PS}} = 0.8$ , the total number of circuits is given by

$$N_{\text{cir}} = N_{\text{PS}} \cdot N_{\text{cir/PS}} + N_{\text{MA}} \cdot \left\lceil \frac{l_{\text{MA}}}{l_{\text{PS}}} \cdot N_{\text{cir/PS}} \right\rceil \quad (3)$$

$$= 16 \cdot N_{\text{cir/PS}} + 4 \cdot \lceil 0.8 \cdot N_{\text{cir/PS}} \rceil$$

where  $N_{\text{cir/PS}}$  is the number of circuits in the 4-km PS, and the parentheses are indicating the ceiling function.<sup>1</sup> Since for each circuit, one PC and one EE system are present,  $N_{\text{cir}}$  also identifies the total number of these devices.

### C. Design Inputs

The circuit design is closely linked to the definition of other accelerator parameters, as, for example, the turnaround time, defined as the time spent between the end of stable beams and the start of the next stable beams period [11]. As discussed in [11], the circuit ramp-up time to (or equivalently ramp-down time from) nominal current was fixed to 20 min, as for the LHC dipole

<sup>1</sup>The ceiling function provides the smallest integer greater than or equal to its input.

TABLE III  
CIRCUIT DESIGN INPUTS

	Input	Operating phase	Motivation
i.1	20 min duration	Ramp-up/down	To limit turnaround time
i.2	1.3 kV to ground	During FPA	To limit voltage withstand level

TABLE IV  
CIRCUIT DESIGN TARGETS

	Target: to minimize the...	Operating phase: during...	Goal: to improve the...
t.1	Total number of circuits	-	Simplicity of design, reliability
t.2	Number of magnets in series in a circuit	-	Training campaign
t.3	Circuit energy	-	Fault scenarios
t.4	Peak voltage of PCs	Ramp-up/down	PC design
t.5	Peak power of PCs	Ramp-up/down	Accelerator power demand
t.6	Discharge time constant $\tau$	FPA	Cryogenic recovery time
t.7	$\int i^2 dt$ (MIITs)	FPA	Diode design
t.8	Busbar copper cross section	FPA	Layout inside the cryostat
t.9	Number of spurious triggers of the QDS	FPA	Availability

TABLE V  
CIRCUIT PARAMETERS FOR DIFFERENT VALUES OF  $N_{\text{cir/PS}}$

$N_{\text{cir/PS}}$	1	3	5	7	LHC
t.1 Total number of circuits	20	60	96	136	8
t.2 Number of magnets in series in a circuit	219	73	44	32	154
t.3 Circuit energy [GJ]	8.2	2.7	1.6	1.2	1.1
t.4 Peak voltage of PCs [V]	1200	400	240	175	150
t.5 Peak power of PCs [MW]	14	4.5	2.7	2.0	1.8
t.6 Discharge time constant $\tau$ [s]	550	180	110	80	100
t.7 $\int i^2 dt/10^6$ (MIITs) [ $\text{MA}^2\text{s}$ ]	$36 \times 10^3$	$12 \times 10^3$	$7 \times 10^3$	$5 \times 10^3$	$7 \times 10^3$
t.8 Busbar copper cross section [ $\text{mm}^2$ ]	600	350	270	230	270

circuits, in order to obtain the desired turnaround time. Another input for the circuit design, already discussed in Section I, is the maximum voltage-to-ground during the FPA that should not exceed 1.3 kV. As summarized in Table III, this is needed to limit the voltage withstand level of the electrical insulation of the magnet that has to be much higher than 2.5 kV given by (1), due to the possible presence of faults in the circuit.

#### D. Design Targets

The circuit design is also closely linked to other accelerator systems, as, for example, PCs. For this reason, a broader perspective than the protection point of view is needed to devise an effective circuit layout. This is shown in Table IV, where different targets considered for the design of the FCC-hh dipole circuits are summarized. The first three targets are related to the circuit layout, targets t.4 and t.5 are linked to the circuit behavior during ramp-up and ramp-down, and targets t.6–t.9 are related to the FPA phase. It is interesting to note the first target is met for  $N_{\text{cir/PS}} \rightarrow 1$ , while all the others (t.2–t.9) are met for high values of  $N_{\text{cir/PS}}$ . This shows, from a qualitative point of

view, that the optimal value of circuits per PS is  $N_{\text{cir/PS}} \gg 1$ . The next section will introduce a circuit layout that meets targets t.1–t.8. The objective t.9 of minimizing the number of spurious triggers of the quench detection system (QDS) will be discussed in Section III.

#### E. Proposed Circuit Layout

Table V shows the target variables of Table IV for different numbers of circuit in the 4-km PS ( $N_{\text{cir/PS}}$ ) and compares them with the parameters of the LHC dipole circuits (right column). The number of dipole circuits in the accelerator is given by (3) and increases as  $N_{\text{cir/PS}}$  increases, while all the other circuit parameters decrease as  $N_{\text{cir/PS}}$  increases. It can be seen that, for the solution with one circuit per PS, the ramp-up of the circuit is critical due to the high voltage and high power of the PCs. In particular, the PC peak voltage is close to the maximum voltage-to-ground budget. The real limit for the circuit design comes, however, from the discharge time constant  $\tau$ , which identifies the time that is needed to safely discharge the circuit after a quench or a fault. For several reasons, the value of this parameter

should not be much higher than 100 s. According to the LHC experience, a larger value of  $\tau$  would have negative implications on the number of secondary quenches<sup>2</sup> and, therefore, on the cryogenic recovery time. It implies a larger cross section of the busbars, and it also has negative consequences in the case of electrical faults, as all circuit devices need to withstand the fault currents for a longer time. The minimum number of circuits per PS that leads to a discharge time constant in the order of 100 s is  $N_{\text{cir/PS}} = 5$ . This translates into a total number of dipole circuits equal to 96. This solution appears as a possible compromise among the excessive circuit complexity (target t.1) and the other targets.

In Table V, the parameters defining the ramp-up (t.4 and t.5) and the FPA (t.6–t.8) have been calculated considering the standard strategies applied to the LHC dipole circuits: constant voltage for the ramp-up and insertion of a resistor for the fast EE. More sophisticated strategies can be used in these two phases. For the ramp-up, an initial ramp with constant voltage can be followed by a ramp with constant power. This allows one to decrease the peak power of the converters. As an example, if the peak voltage of the converter is doubled at low current, the circuit can be ramped-up in the same time (20 minutes) with almost half of the peak power in Table V.

For the FPA phase, one might consider extracting the energy with an active load keeping a constant voltage during the discharge, i.e., linearly decreasing the current [12]. When the current discharge is linear, it is possible to show that the discharge time constant (intended as the time to reach 37% of the initial current) is reduced by 37% with respect to one of the exponential discharges provided by the resistor. The resulting MIITs is reduced by 33%. This means that, when the active EE technique is applied, a number  $N_{\text{cir/PS}} = 3$  is sufficient to have a discharge time constant of about 115 s. The total number of circuits is significantly reduced, but the subdivision of the PS into multiple circuits is still needed.

#### F. Additional Considerations

The numbers presented in the previous section are obtained considering the parameters of the  $\cos-\theta$  magnet listed in Table I. The block-coil design has similar parameters, which lead to the same circuit layout. The common-coil and canted  $\cos-\theta$  magnets are characterized by a significantly smaller inductance (achieved through a higher nominal current), which provides an advantage from the circuit point of view. Considering the same inputs in Table III and the standard EE technique by means of a resistor, the subdivision of the PS into four circuits ( $N_{\text{cir/PS}} = 4$ ) is sufficient to ensure a discharge time constant of about 110 s. The total number of dipole circuits for the FCC-hh is, therefore, reduced from 96 for the  $\cos-\theta$  and block-coil to 80 for the common-coil and canted  $\cos-\theta$ . The main disadvantage for the last two magnet types is that all the circuit elements need to be designed for a higher nominal current. As an example, the busbar copper cross section increases by 50% (from 270 to 400 mm<sup>2</sup>).

<sup>2</sup>Number of neighboring magnets that are quenched after one magnet is quenched due to the thermal propagation in the helium.

TABLE VI  
POSSIBLE ELECTRICAL FAULTS AND EXPECTED CONSEQUENCES FOR THE FCC-HH DIPOLE CIRCUITS

Fault type	Tolerance capability	Main consequences
Single short-to-ground	Yes	Circuit voltage-to-ground doubled
Multiple shorts-to-ground or short-circuit	No	Overcurrent through the short path Distributed uncontrolled energy release
Open circuit in a section protected by the diode	Yes	Confined uncontrolled energy release
Open circuit elsewhere	No	Overvoltages and arcs Distributed uncontrolled energy release

Another important consideration is that the proposed circuit layout is obtained starting from the requirements on the nominal operation. A dedicated study is needed to investigate the possible fault scenarios and improve circuit reliability. Such a study is beyond the scope of this article. Nevertheless, the main electrical faults that could occur in the FCC-hh dipole circuit can be discussed here along with the capability of the circuit to tolerate them.

As shown in Table VI, the circuit can tolerate a single short-to-ground if the nominal grounding point is connected through a fuse. In the presence of a short-to-ground, the fuse is blown, and the circuit voltage-to-ground is doubled. The total voltage-to-ground seen by the magnets is, according to (1),  $\hat{V}_{\text{magnet, gnd}} = 1.2 \text{ kV} + 2 \cdot 1.3 \text{ kV} = 3.8 \text{ kV}$ . Magnets have to be designed to withstand a voltage larger than this value. The circuit cannot tolerate multiple shorts-to-ground or, equivalently, a short connecting two points with different voltage since this would generate a current loop alternative to the healthy circuit. In this case, magnets and circuit elements belonging to the fault path cannot be protected. An open circuit can be tolerated if it occurs in a circuit section protected by the bypass diode. The energy stored in the fault path is locally released in an uncontrolled way, but, thanks to the diode, the rest of the circuit is subject to normal voltage values. This is not the case if the open circuit occurs in a section that is not protected by the bypass diode. This last fault would imply a distributed and uncontrolled energy release with a high potential to damage the circuit. For this reason, the circuit elements belonging to these parts must be designed and tested to minimize the possibility of open circuits, for example, by means of redundancy.

### III. SPURIOUS QDS TRIGGERS

#### A. Adopted Numerical Model

In the previous section, a layout was proposed for the FCC-hh dipole circuit as a result of the considered input parameters and a compromise among the identified targets. Numerical simulations are needed to test the circuit behavior during the most critical FPA phase. Fig. 5 shows the schematic of the FCC-hh dipole circuit. It features 44 dipole magnets connected in series, one PC with parallel thyristor crowbar, and one EE system grounded in its midpoint. A CLIQ protection system has to be connected to each magnet to protect it in the case

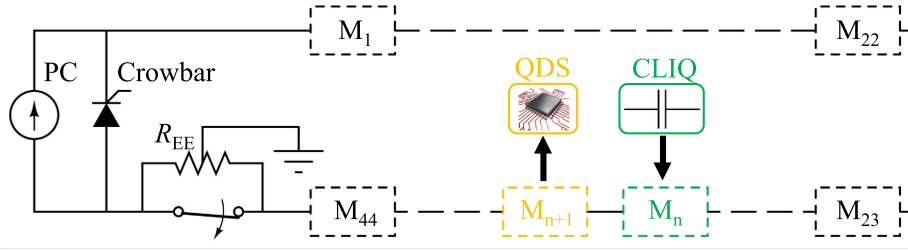


Fig. 5. Schematic of the proposed FCC-hh dipole circuit layout with 44 magnets in series. The presence of the CLIQ protection system and the QDS is also highlighted on the two generic magnets  $M_n$  and  $M_{n+1}$ .

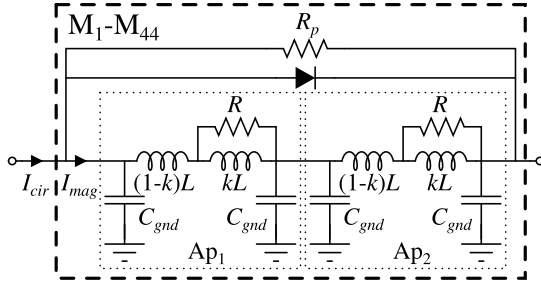


Fig. 6. Schematic of the lumped element model adopted for magnets from  $M_1$  to  $M_{44}$  except for  $M_n$  and  $M_{n+1}$ .

of a quench [2]. CLIQ is triggered by the QDS that is also monitoring each magnet. The last target of the circuit design identified in Table IV is to minimize the number of spurious triggers of the QDS in order to maximize the availability of the FCC. As already observed in the LHC, the switching OFF of the PC and the insertion of the EE system generates voltage transients in the circuit [13]. The probability of spurious triggers derives from the transients amplitude and the sensitivity of the quench detection signal on the transients [14].

In order to study this problem in detail, a numerical model that considers the circuit domain, the magnet electrothermal domain, the CLIQ protection system, and the QDS was developed. The circuit of Fig. 5 was modeled by means of a Cadence PSpice netlist, where all magnets except  $M_n$  and  $M_{n+1}$  implement the lumped element model already developed in [15] and shown in Fig. 6. The model considers that each magnet has a parallel diode to bypass the circuit current in the case of quench ( $I_{mag} < I_{cir}$ ) and a resistor to limit the amplitude of voltage transients. In order to limit the leakage current flowing through the resistor during the ramp-up to values similar to those in the LHC, the parallel resistance has been set to  $R_p = 500 \Omega$ . The capacitance-to-ground of the FCC-hh cos- $\theta$  magnet was estimated by means of an FE electrostatic model and found to be  $C_{gnd} = 90$  nF. Moreover, the inductive and resistive elements in the circuit of Fig. 6, modeling the effects of eddy currents [13], [15], were estimated by means of a COMSOL electrothermal magnet model solving for the interfilament coupling currents [7] and found to be  $L = 283$  mH,  $k = 0.46$ , and  $R = 39 \Omega$ .

Magnet  $M_n$  in Fig. 5 is subject to a quench and to the subsequent activation of the CLIQ protection system. Fig. 7 shows its lumped element circuit model. The voltage across the two electrical parts (Ep) of each magnet aperture (Ap) is

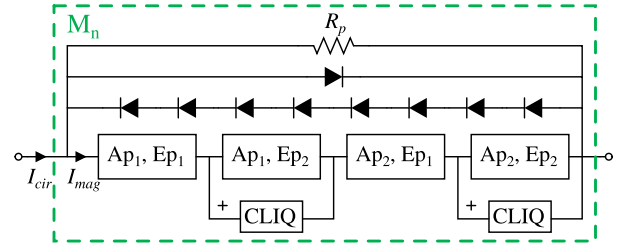


Fig. 7. Schematic of the lumped element model adopted for the quenching magnet  $M_n$ . The voltage across the two electrical parts (Ep) of each magnet aperture (Ap) is provided by the COMSOL electrothermal model [7].

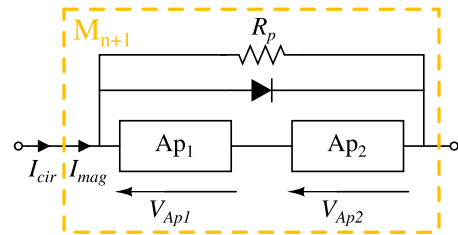


Fig. 8. Schematic of the lumped element model adopted for the magnet  $M_{n+1}$ . The voltage across the two magnet apertures (Ap) is provided by the COMSOL electrothermal model [7].

provided by the COMSOL electrothermal model [7], through a field-circuit coupling algorithm implemented by the STEAM cosimulation framework [8]. The use of CLIQ requires a series of backward diodes connected in parallel to the magnet [6], as shown in Fig. 7. Their function is to provide a continuity path for the current when  $I_{mag} > I_{cir}$  due to current oscillations induced by CLIQ. More than one diode is needed to have a total threshold voltage that is higher than the magnet voltage obtained during EE. For the FCC-hh circuit, this voltage is given by  $V_{mag,EE} = V_{EE}/N_{mag} = 2 \cdot V_{circuit,gnd}/N_{mag} \cong 60$  V.

The reaction of the QDS to the voltage transients is checked on the neighboring magnet  $M_{n+1}$  (see Fig. 5). The selection of this magnet is justified by observations of the LHC dipole circuits, which show that, once a magnet quenches, its neighbors are the most vulnerable to spurious triggers. Fig. 8 shows its lumped element circuit model. The voltage across the two magnet apertures (Ap) is provided by the COMSOL electrothermal model [7]. The model can consider perfectly balanced apertures or, as already observed in the LHC dipole magnets, apertures with slightly different frequency response [13]. The difference of the two aperture voltages is considered as the input of the QDS

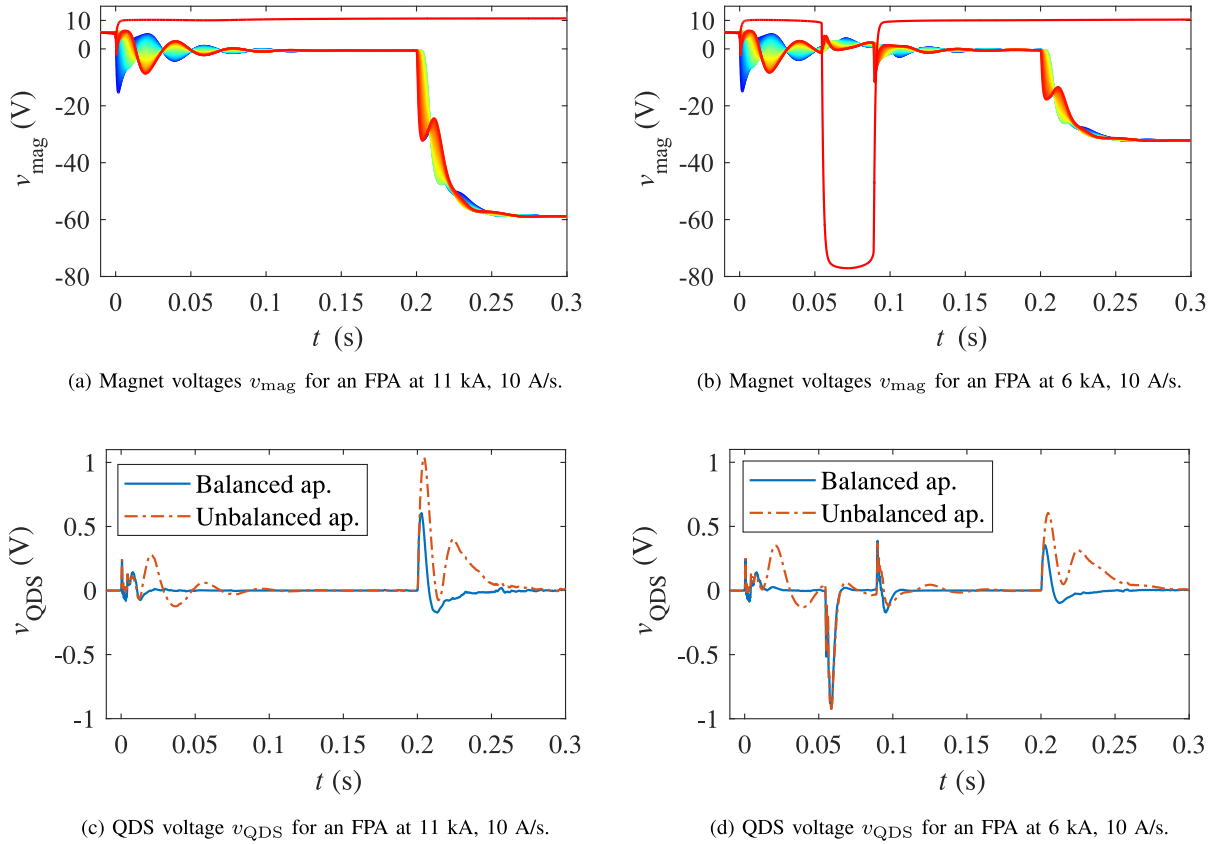


Fig. 9. (a) and (b) Voltage across the magnets: each magnet has a different color ranging from blue (magnet 1) to red (magnet 44). (c) and (d) Differential voltage across the apertures of magnet 44 for balanced apertures (blue trace) and unbalanced apertures (red dash-dotted trace).

( $v_{\text{QDS}} = v_{\text{Ap1}} - v_{\text{Ap2}}$ ). As in the LHC QDS system [16], when the differential voltage is larger than a threshold for a period longer than the discrimination time, a quench is detected and the protection systems are activated.

## B. Results

The circuit layout described in the previous section was simulated considering different positions in the chain for magnets  $M_n$  and  $M_{n+1}$ . The highest differential voltage was obtained for position  $n = 43$ , i.e., for the QDS of the magnet close to the PC and EE systems, which are the origin of the voltage transients in the circuit. The simulation considered an FPA occurring during the ramp-up of the circuit with a nominal ramp rate of 10 A/s and at different current levels. Two worst cases were observed: the FPA at a nominal current of 11 kA and the FPA at a lower current of 6 kA. Fig. 9 shows the voltage across all magnets ( $v_{\text{mag}}$ ) and the differential voltage across the apertures of magnet 44 ( $v_{\text{QDS}}$ ) for these two cases.

Fig. 9(a) shows the magnet voltages obtained for an FPA at a current level of 11 kA. At  $t = 0$  s, a quench is detected on magnet 43, the PC is turned OFF, and CLIQ is activated. The voltage across magnet 43 is equal to the forward diode voltage [red trace in Fig. 9(a)]. The voltage across the other magnets is subject to oscillations that occur after both the shutdown of the PC ( $t = 0$  s) and the activation of the EE system ( $t = 0.2$  s). Fig. 9(c) shows the differential voltage  $v_{\text{QDS}}$  across the apertures

of magnet 44 in the case of perfectly balanced apertures (blue trace) and unbalanced apertures (red trace). The unbalanced case was obtained by increasing the resistivity of the cable copper matrix in one of the two apertures of the COMSOL model by 50%. This is compatible with the unbalance observed in the LHC dipole magnets [13].  $v_{\text{QDS}}$  shows relatively large oscillations when compared to the foreseen quench detection thresholds, especially for the case of unbalanced apertures. For comparison, the threshold and the discrimination time of the LHC QDS system are 100 mV and 10 ms, respectively [16]. These oscillations might produce unwanted triggers of the QDS.

Fig. 9(b) and (d) shows the voltages obtained for an FPA at a current level of 6 kA. The oscillations of  $v_{\text{mag}}$  and  $v_{\text{QDS}}$  after the PC switching OFF ( $t = 0$  s) are similar to the ones in Fig. 9(a) and (c), as the ramp rate and the voltage across the PC are the same. On the other hand, the oscillations of  $v_{\text{mag}}$  and  $v_{\text{QDS}}$  after the EE insertion ( $t = 0.2$  s) are smaller than the ones in Fig. 9(a) and (c), since the voltage across the resistance of the EE system is lower due to the lower current level. Additional transients are obtained at  $t \cong 0.06$  s and  $t \cong 0.09$  s due to the CLIQ system protecting magnet 43. When CLIQ is fired at the operating current of 6 kA,  $I_{\text{mag}}$  in Fig. 7 becomes greater than  $I_{\text{cir}}$  for  $0.06 \text{ s} \leq t \leq 0.09 \text{ s}$ , and the backward diodes are activated. In the simulation, the threshold voltage of the series of backward diodes is 80 V. As shown in Fig. 9(d), this generates additional oscillations of  $v_{\text{QDS}}$  similar to the ones introduced by the PC switching OFF and EE system activation. In other words, the operation of the CLIQ

protection system in a circuit of magnets adds disturbances to the QDS signal but does not significantly increase the probability of spurious triggers.

#### IV. CONCLUSION

This article proposes a conceptual design for the dipole circuits of the FCC-hh. Two inputs drive the design, namely, a ramp-up and ramp-down time of 20 min, to limit the turnaround time of the machine, and a maximum circuit voltage-to-ground of 1.3 kV during the FPA, to limit the voltage withstand level. Additional targets are included to take into account the tunnel layout and the FCC-hh operation. This article proposes to employ a superconducting link to locate PCs and EE systems, bulky devices often subject to maintenance, close to the access points. The proposed circuit layout results as a compromise between the two most limiting factors: on the one hand, the reduction of the total number of dipole circuits in order to limit the complexity and improve the reliability of the circuit system, and, on the other hand, the reduction of the circuit discharge time, which gives many advantages, such as, for example, the reduction of the cryogenics recovery time. Starting from the experience on the LHC dipole circuits, the compromise is identified as the minimum number of circuits that leads to a discharge time constant in the order of 100 s. In total, 96 circuits are needed to power the  $\cos\theta$  and block-coil dipole magnets, while 80 circuits are needed for the common coil and canted  $\cos\theta$  dipole magnets.

By means of numerical simulations, this article also shows the response of the proposed circuit layout during the critical FPA phase. The PC switching OFF and the insertion of the EE system provoke large oscillations in the magnets voltage that could induce spurious triggers of the QDS. This article shows that the amplitude of the oscillations is tightly coupled with the uniformity of the cable parameters across the two magnet apertures. Therefore, one possibility to reduce them is through a tight control of the cable parameters during production.

The simulations also indicate that the CLIQ protection system introduces additional voltage oscillations, whose amplitude is similar to the ones provoked by the insertion of the EE system. This implies that the protection system can be easily integrated into the proposed circuit layout without increasing the probability of spurious triggers of the quench detection units. In conclusion, this article shows that CLIQ can be effectively employed to protect the entire string of FCC-hh dipole magnets.

#### ACKNOWLEDGMENT

The authors would like to acknowledge R. Schmidt and A. Siemko of the Machine Protection and Electrical Integrity Group, CERN, for the fruitful discussions on the optimization of the circuit layout.

#### REFERENCES

- [1] D. Tommasini *et al.*, "Status of the 16 T dipole development program for a Future Hadron Collider," *IEEE Trans. Appl. Supercond.*, vol. 28, no. 3, Apr. 2018, Art. no. 4001305.
- [2] M. Prioli *et al.*, "The CLIQ quench protection system applied to the 16 T FCC-hh dipole magnets," *IEEE Trans. Appl. Supercond.*, 2019.

- [3] T. Salmi *et al.*, "Quench protection analysis integrated in the design of dipoles for the Future Circular Collider," *Phys. Rev. Accel. Beams*, vol. 20, no. 3, 2017, Art. no. 032401.
- [4] T. Salmi *et al.*, "Suitability of different quench protection methods for a 16 T block-type Nb3Sn accelerator dipole magnet," *IEEE Trans. Appl. Supercond.*, vol. 27, no. 4, Jun. 2017, Art. no. 4702305.
- [5] F. Rodriguez-Mateos and F. Sonnemann, "Quench heater studies for the LHC magnets," in *Proc. Particle Accel. Conf.*, 2001, vol. 5, pp. 3451–3453.
- [6] E. Ravaoli, "CLIQ," Ph.D. dissertation, Univ. Twente, Enschede, The Netherlands, 2015. [Online]. Available: <http://doc.utwente.nl/96069/>
- [7] L. Bortot *et al.*, "A 2-D finite-element model for electrothermal transients in accelerator magnets," *IEEE Trans. Magn.*, vol. 54, no. 3, Mar. 2018, Art. no. 7000404.
- [8] L. Bortot *et al.*, "STEAM: A hierarchical cosimulation framework for superconducting accelerator magnet circuits," *IEEE Trans. Appl. Supercond.*, vol. 28, no. 3, Apr. 2018, Art. no. 4900706.
- [9] L. Bortot *et al.*, "A consistent simulation of electrothermal transients in accelerator circuits," *IEEE Trans. Appl. Supercond.*, vol. 27, no. 4, Jun. 2017, Art. no. 4001305.
- [10] I. C. Garcia *et al.*, "Optimized field/circuit coupling for the simulation of quenches in superconducting magnets," *IEEE J. Multiscale Multiphys. Comput. Techn.*, vol. 2, pp. 97–104, 2017.
- [11] R. Alemany Fernandez *et al.*, "FCC-hh turn-around cycle," CERN, Geneva, Switzerland, Tech. Rep. CERN-ACC-2016-0341, Jul. 2016. [Online]. Available: <https://cds.cern.ch/record/2239138>
- [12] V. D. Karavantzis, J. Biela, and F. Rodriguez Mateos, "Optimized design of a novel energy extraction system for superconducting magnets in future particle accelerators," in *Proc. 21st Eur. Conf. Power Electron. Appl.*, 2019.
- [13] E. Ravaoli, K. Dahlerup-Petersen, F. Formenti, J. Steckert, H. Thiesen, and A. Verweij, "Modeling of the voltage waves in the LHC main dipole circuits," *IEEE Trans. Appl. Supercond.*, vol. 22, no. 3, Jun. 2012, Art. no. 9002704.
- [14] E. Ravaoli *et al.*, "Impact of the voltage transients after a fast power abort on the quench detection system in the LHC main dipole chain," *IEEE Trans. Appl. Supercond.*, vol. 22, no. 3, Jun. 2012, Art. no. 9002504.
- [15] R. Shafer, "Eddy currents, dispersion relations, and transient effects in superconducting magnets," FERMILAB, Batavia, IL, USA, Tech. Rep. FERMILAB-TM-0991, 1980.
- [16] R. Denz, "Electronic systems for the protection of superconducting elements in the LHC," *IEEE Trans. Appl. Supercond.*, vol. 16, no. 2, pp. 1725–1728, Jun. 2006.

**Marco Prioli** was born in Cesena, Italy, in 1986. He received the M.Sc. and Ph.D. degrees in electrical engineering from Politecnico di Milano, Milano, Italy, in 2010 and 2014, respectively.

From 2014 to 2015, he was a Research Assistant with the Dipartimento di Elettronica, Informazione e Bioingegneria, Politecnico di Milano, where he was involved in the field of electrical measurements and uncertainty evaluation. In 2015, he joined the Machine Protection and the Electrical Integrity Group, CERN, Geneva, Switzerland, where he worked on the protection of superconducting magnets and circuits of present and future particle colliders. He is currently with the Istituto Nazionale di Fisica Nucleare, Milano, where he is involved in the development of the prototypes of the high-order corrector magnets for the High-Luminosity Large Hadron Collider project and the following production phase.

**Bernhard Auchmann** was born in Vienna, Austria. He received the Diploma and Ph.D. degree in electrical engineering from the Vienna University of Technology, Vienna in 2001 and 2004, respectively.

Since 2005, he has been a scientific staff with CERN, Geneva, Switzerland. Among others, his responsibilities covered the development of software for the electromagnetic design of accelerator magnets, the electromechanical design of high-field magnets, and the development and application of multiphysics simulation software to model transient phenomena in circuits of superconducting magnets. Since 2016, he has also been with the Paul Scherrer Institute, Villigen, Switzerland, leading the Swiss Accelerator Research and Technology) superconducting magnet R&D for the Future Circular Collider.

**Lorenzo Bortot** received the M.Sc. degree in electrical engineering from the Università degli Studi di Padova, Padova, Italy, in 2012. He is currently working toward the Ph.D. degree in a collaboration project between CERN, Geneva, Switzerland, and the Technische Universität Darmstadt, Darmstadt, Germany, working on the development of numerical models for high-temperature superconducting magnets.

From 2015 to 2018, he was a Research Fellow with the Technology Department, CERN, where he dealt with numerical analysis of the magnetothermal transients and superconducting accelerator circuits. His research interests are mainly focused on the use of the finite-element method in the analysis of safety-critical transient phenomena in superconducting accelerator magnets.

**Michał Maciejewski** was born in Jastrzębie-Zdrój, Poland. He received the M.Sc. and Ph.D. degrees in automatic control and robotics from the Łódź University of Technology, Łódź, Poland, in 2014 and 2019, respectively.

In 2013, he joined Machine Protection and the Electrical Integrity Group, CERN, Geneva, Switzerland, where he currently is a Senior Research Fellow. His main research activities include the development of simulation software for magnetothermal and electrical simulation of superconducting magnets and circuits, and performance evaluation of quench protection systems of the Large Hadron Collider and its upgrades. His research interests include numerical methods, cooperative simulation, scientific computing, machine learning, and port-Hamiltonian modeling.

**Tiina Salmi** received the M.Sc. degree in quench protection of a fast-cycled superferic magnet from CERN, Geneva, Switzerland, in 2009, and the Ph.D. degree from the Tampere University of Technology, Tampere, Finland, in 2015.

Since 2009, she has been working with various aspects related to accelerator magnet quench protection. During her Ph.D. research, she spent three years with the Lawrence Berkeley National Laboratory, Berkeley, CA, USA, to study heater-based protection applied to the Large Hadron Collider luminosity upgrade quadrupoles. During the Future Circular Collider (FCC) project, she was a Postdoctoral Researcher funded by the Academy of Finland at Tampere University and studied the quench protection of the FCC 16-T dipole magnets.

**Arjan Verweij** received the M.Sc. degree in applied physics and the Ph.D. degree in electrodynamics of superconducting Rutherford cables in accelerator magnets in 1991 and 1995, respectively, from the University of Twente, Enschede, The Netherlands.

As a Postdoctoral Researcher with CERN, Geneva, Switzerland, for three years, he designed and constructed the FRESKA test facility for the electrical characterization of superconducting cables up to 10 T, 32 kA, and down to 1.9 K. He was then awarded a staff contract at CERN in 1998, following up the production and quality control of superconducting strands and cables for the Large Hadron Collider (LHC), as well as performing and analyzing many tests on Nb-Ti magnets. In 2007, he was strongly involved in the protection, operation, and performance of the 1700 superconducting circuits in the LHC. Since 2015, he has been leading the Performance and Evaluation Section, Machine Protection and Electrical Integrity Group, Technology Department, CERN, where he is responsible for a wide range of R&D, studies, simulations, experiments, and data analysis aiming to further enhance the operational performance of the LHC and future accelerators.